*Sensors and Materials*, Vol. 34, No. 5 (2022) 1649–1663
MYU Tokyo



S & M 2917

# Decomposition System That Automatically Tracks Ammonia Concentration

Sheng-Yi Tang* and Yu-Hao Hu

Department of Power Mechanical Engineering, National Formosa University,
No. 64, Wunhua Rd., Huwei Township, Yunlin County 632, Taiwan, R.O.C.

(Received November 6, 2021; accepted March 30, 2022)

***Keywords:*** ozone, ceramic plate type, ozone generator, ammonia, ammonia gas detector

In 2020, East Asia was officially declared free of foot-and-mouth disease, which means that the number of piggeries in the region will increase. Piggeries produce ammonia gas that must be managed. In this study, we propose a decomposition system that automatically tracks ammonia concentration and employs ozone and water mist to decompose ammonia gas. The key components of the system are a ceramic plate-type ozone generator, an ammonia gas detector (e.g., MQ-137), and an ammonia tracking circuit. The oxygen generator consists of two parts, namely, the circuit architecture and the oxygen supply. The circuit architecture consists of an AC power supply, a standby power supply, an electromagnetic interference filter, a power factor correction circuit of a boost converter, a full-bridge parallel resonance converter, a full-bridge drive circuit, and a ceramic plate. The system operates by inputting ozone of varying concentrations into the washing basket to mix with mist and ammonia gas. A voltage signal from the ammonia tracking circuit is used as the basis for adjusting the operating frequency of the ozone generator and the resonance voltage. The ozone generator can output four power levels (25, 50, 75, and 100%), which correspond to four different ozone concentrations. The experimental results demonstrated that decomposition was most effective when the ozone generator output power was 100%.

## 1. Introduction

In 1997, East Asia experienced an outbreak of foot-and-mouth disease, which hindered the region from exporting pork and prompted a reduction in the number of piggeries. After decades of effort, East Asia was finally certified by the Office International des Epizooties as free of foot-and-mouth disease in 2020. This means that East Asia's pork will soon return to the international market and the demand for piggeries will substantially increase. Piggeries generate a large amount of ammonia gas that severely lowers air quality. When an environment has too much ammonia gas, the ecosystem acidifies and eutrophicates. Ammonia gas is also abrasive to the respiratory tract of humans. When ammonia gas reaches a certain concentration, it causes tracheal burns, airway obstruction, and alveolar edema.[1] In the lymphatic system, it can

*Corresponding author: e-mail: arthurta@nfu.edu.tw
https://doi.org/10.18494/SAM3805

ISSN 0914-4935 

increase the number of blood cells and cause ariboflavinosis and pulmonary artery thrombosis. In the cardiovascular system, it can cause increased blood pressure, increased pulse rate, and even cardiac arrest.[2] In the gastrointestinal system, it can cause edema and burns on the esophagus, lips, and throat.[3] Therefore, the concentration of ammonia gas around a piggery severely affects the health of nearby residents.

Common existing deodorization methods involve the use of hypochlorous acid water (bleach), activated carbon, and ozone. (1) Hypochlorous acid water is a chemical agent that can easily cause environmental pollution and metal corrosion. (2) Activated carbon absorbs odor, but it is a consumable. After it is saturated with odor, it must be disposed, and its waste causes severe environmental pollution. (3) Ozone is a natural deodorant. When ozone reacts with ammonia gas, it is immediately reduced to oxygen, so using it can avoid introducing secondary pollution into the environment. To date, ozone has been widely applied in the food processing industry and in the agriculture, fishing, and animal husbandry industries. Ozone can naturally reduce. When it is used as a disinfectant, it does not leave any residue in food products, unlike other bactericides and disinfectants. Therefore, it has gradually been used to replace chemical agents such as hydrogen peroxide and hypochlorous acid water.[4–9]

According to a relevant study,[10] ammonia gas contains a large amount of hydrogen. When heated at high temperatures, ammonia gas degrades and can be used to generate hydrogen for fuel cells. Ammonia gas detectors (e.g., MQ-137) have been widely used to detect the ammonia generated from manure at livestock farms or from rotting food, which is caused by microbes.[11–13] The MQ-137 detector uses analog circuits to convert ammonia concentrations into voltage signals. Subsequently, it uses an analog–digital converter to transform voltage signals into digital signals to indicate the ammonia concentration. In this study, we propose a degradation system that automatically tracks the ammonia concentration and simultaneously mixes ammonia gas, high-concentration ozone, and water mist to eliminate the odor of ammonia. An MQ-137 detector was installed at the air outlet of the system to detect the presence of ammonia; when ammonia was detected, the system increased the ozone concentration.

The existing ozone production equipment has the following disadvantages. (1) The quartz tube uses a conventional transformer to generate ozone using a high voltage (14 kV) and a low frequency (60/50 Hz). Because the conventional transformer has a low operating frequency and a low efficiency, the generated ozone is of low concentration, approximately 53 g/m$^3$ (26997 ppm). (2) To date, feedback control has not been successfully utilized to precisely control the ozone output concentration. The ozone output concentration can only be controlled by turning the system fully on or off, resulting in numerous inconveniences in application. Sites that require precise concentration control consequently cannot use ozone equipment.[14–16] Therefore, in this study, we propose a decomposition system that automatically tracks the ammonia concentration (DSATAC). The following sections describe the DSATAC and the structure and circuit parameter design of the ceramic plate-type ozone generator (CPOG) and ammonia tracking circuit (ATC), as well as an ammonia concentration decomposition experiment.

## 2. Architecture of DSATAC

As shown in Fig. 1, the DSATAC has three internal paths connected to the washing basket for ozone, ammonia gas, and water mist to mix so that the ammonia gas will decompose. (1) The ozone input path consists of an oxygen machine, a CPOG, and an ozone analyzer. (2) The input path of ammonia gas consists of a fixed quantity of ammonia water to generate ammonia gas, a flow meter, and an air pump. (3) The water mist input path consists of a water storage bucket, a spray machine, and a water mist blow head. The three paths are input into a 10 L washing basket for mixing. The ATC measures the decomposed ammonia gas concentration in real time. It transmits a voltage signal ($v_{Ammonia}$) to adjust the operating frequency and resonance voltage of the CPOG depending on the ammonia concentration, thereby controlling the four output powers of the CPOG (25, 50, 75, and 100%), which correspond to four ozone concentrations (30.8, 54.2, 73.6, and 90.5 ppm). Subsequently, the ozone analyzer measures the ozone concentration in real time and provides a voltage feedback signal ($v_{Ozone}$) to the CPOG to precisely control the ozone concentration. Table 1 provides the specifications of the key components of the DSATAC. In the next section, we describe the structure, circuit, and design of the DSATAC.

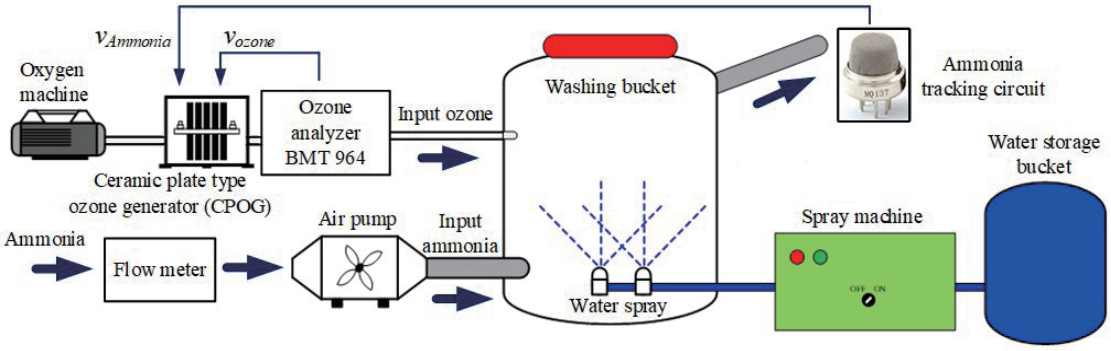


Fig. 1. (Color online) DSATAC.

Table 1
Key devices in the decomposition system that automatically tracks ammonia concentration.

| Device | Model | Specification |
|---|---|---|
| Ceramic plate-type ozone generator | KT-Module10 | Max. ozone concentration = 145 g/m$^3$ at 2 LPM |
| Oxygen machine | IRC5PO2V | Max. flow = 5 LPM |
| Air pump | DY-50-A | Max. flow = 50 LPM<br>Rated pressure = 12 kPa |
| Spray machine | SF-5248-800 | Max. flow = 4.8 LPM<br>Pressure range = 170–200 psi |
| Ozone analyzer | BMT 964 | Max. measuring ozone concentration = 254687 ppm ± 0.4% |
| Ammonia sensor | MQ-137 | Max. measuring ammonia concentration = 500 ppm ± 0.2% |

### 2.1 Architecture of CPOG

As demonstrated in Fig. 2, the CPOG is divided into two parts, namely, the circuit structure and the oxygen supply. The circuit structure consists of an AC source, standby power, power factor correction (PFC), a full-bridge resonant inverter (FBRI), a full-bridge control circuit (FBCC), and a ceramic plate. Among them, the PFC, FBRI, and FBCC are high-voltage drive devices (blue blocks) that drive the ceramic plate. After the three voltage feedback signals $v_{cr\_sen}$, $v_{Ozone}$, and $v_{Ammonia}$ are input to the FBCC to alter the operational frequency and to output pulse-width modulation (PWM) to control the FBRI operational frequency and resonance voltage, four power levels are output (25, 50, 75, and 100%) depending on the input. After air enters the oxygen machine, it is split into nitrogen and oxygen. Nitrogen is released into the environment, and oxygen is input to the ceramic plate. The ceramic plate generates a microdischarge reaction. Through ionic processes and free radical reactions, high-concentration oxygen produces oxygen radicals that eventually form ozone.[17] Because the high-voltage drive module plays a critical role in the CPOG, the next section describes the circuit parameter design of the high-voltage drive device.

### 2.2 Circuit parameter design of high-voltage drive device

As shown in Fig. 3, the high-voltage drive device consists of a PFC, FBPR, and FBCC. The PFC adopts a boost converter, which produces an output voltage higher than the input voltage; the voltage after the bridge rectifier, the power switch, and the output capacitance have a common ground. The control circuit has a simple design, and the output voltage can be set to a large range. It offers an ideal selection for high-voltage loading. The FBRI consists of choke inductance, a metal oxide semiconductor field-effect transistor (MOSFET) ($Q_1$–$Q_4$), an FBCC, an ATC, a gate driver (UCC27712),[18] resonance inductance ($L_{r1}$), resonance capacitance ($C_{r1}$), and a step-up transformer (TR). In this study, we used a Texas Instruments (TI) UCC28019 controller to drive the boost converter, which operates under the continuous conduction mode with average current control.[19] On the basis of the specifications of the PFC (Table 2), the key

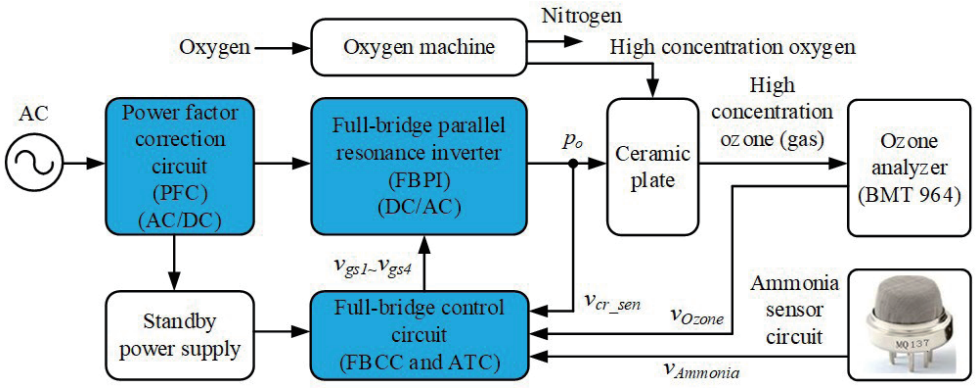


Fig. 2. (Color online) CPOG.

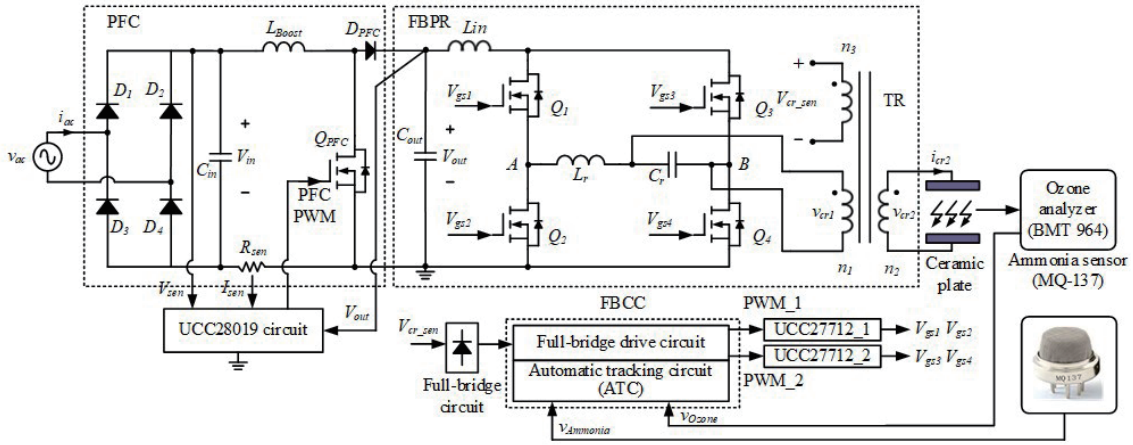


Fig. 3. (Color online) High-voltage drive device.

Table 2
Boost converter specifications.

| Symbol | Value | Unit |
|---|---|---|
| $V_{ac(min)} - V_{ac(max)}$ | 90–240 | V |
| $f_{Line}$ | 47–63 | Hz |
| $\Delta V_{Ripple}$ | 6 | % |
| $\Delta I_{Ripple}$ | 20 | % |
| $V_{in\_Rectified\_min}$ | 127 | V |
| $V_{out}$ | 390 | V |
| $I_{out}$ | 0.8 | A |
| $P_{out}$ | 300 | W |
| $f_{sw}$ | 65 | kHz |
| $t_{Holdup}$ | 20 | ms |
| $V_{out\_holdup}$ | 312 | V |
| $PF$ | 0.95 | — |
| $\eta_{PFC}$ | 0.9 | — |

circuit parameters of the PFC are considered to be the maximum duty cycle ($D_{(max)}$), input voltage ripple ($V_{Ripple}$), input current ripple ($I_{Ripple}$), input capacitance ($C_{in}$), output capacitance ($C_{out}$), and energy storage inductance ($L_{Boost}$). According to the literature,[20] first, we used Eq. (1) to input the input voltage of the minimum alternation $V_{ac(min)}$ = 90 V and the output voltage $V_{out}$ = 390 V to calculate and arrive at $D_{(max)}$ = 0.67. According to Eq. (2), we calculated the input voltage ripple $V_{Ripple}$ = 7.62 V, meaning that the alteration range of $V_{ac(min)}$ is 82.38–97.62 V. Next, we used Eqs. (3) and (4) to respectively calculate the input current $I_{in}$ = 5.51 A and input ripple current $I_{Ripple}$ = 1.10 A, meaning that $I_{in}$ has an alteration range of 4.41–6.61 A. Finally, we used Eqs. (5)–(7) to calculate $C_{in} \leq 0.28$ μF, $C_{out} \leq 219$ μF, and $L_{Boost} \leq 1.2$ mH. The actual values used were $C_{in}$ = 0.33 μF, $C_{out}$ = 270 μF, and $L_{Boost}$ = 1.3 mH.

$$D_{(max)} = \frac{V_{out} - \left(\sqrt{2}V_{ac(min)}\right)}{V_{out}} \tag{1}$$

$$V_{Ripple} = \Delta V_{Ripple} \times \left( \sqrt{2} V_{ac(min)} \right) \tag{2}$$

$$I_{in} = \frac{\sqrt{2} P_{out}}{\eta \times V_{ac(min)} \times PF} \tag{3}$$

$$I_{Ripple} = \Delta I_{Ripple} \times I_{in} \tag{4}$$

$$C_{in} \geq \frac{I_{Ripple}}{8 \times f_{sw} \times V_{Ripple}} \tag{5}$$

$$C_{out} \geq \frac{2 P_{out} t_{Holdup}}{V_{out}{}^2 - V_{out\_holdup}{}^2} \tag{6}$$

$$L_{Boost} \geq \frac{V_{out} D(1-D)}{f_{sw} I_{Ripple}} \tag{7}$$

Figure 3 and Table 3 present the FBRI and electrical specifications, respectively. When $Q_1$ and $Q_4$ are conducted and $Q_2$ and $Q_3$ are cut off, $V_{AB} = V_{in}$. By contrast, when $Q_1$ and $Q_4$ are cut off and $Q_2$ and $Q_3$ are conducted, $V_{AB} = -V_{in}$. Under the cycle of the two, $V_{AB}$ forms an AC square-wave voltage working on $L_r$ and $C_r$. At this moment, $C_r$ generates a high sine-wave voltage ($V_{cr1}$). Through the step-up TR, the sine-wave voltage increases again to 4–5 kV, which drives the ceramic plate. Its major circuit parameters are $L_r$, $C_r$, and $V_{cr1\_max}$. Using the specifications listed in Table 3 and those in the literature,[21] first, we used Eqs. (8) and (9) to calculate the corner frequency $\omega_o$ = 275 krad/s and load resistance $R_{Load}$ = 357.5 Ω. Therefore, we knew the operational frequency and load conditions suitable for driving the ceramic plate. Next, we used Eqs. (10) and (11) to calculate $L_r$ = 0.52 mH and $C_r$ = 20.2 nF, respectively. The actual values adopted were $L_r$ = 0.6 mH and $C_r$ = 22 nF. Finally, using Eq. (12), we calculated

Table 3
FBRI specifications.

| Symbol | Value | Unit |
|---|---|---|
| $V_{in}$ | 390 | V |
| $P_{Load}$ | 250 | W |
| $f_r$ | 46.9 | kHz |
| $\omega_r$ | 294 | krad/s |
| $Q_L$ | 2.5 | — |
| $\eta_{FBRI}$ | 0.9 | — |
| Duty ratio | 0.49 | — |
| $n_1$:$n_2$:$n_3$ | 1:4:0.05 | — |

and obtained $V_{cr1\_max}$ = 1242 V. By using the TR $n_2$ = 4, $V_{cr1\_max}$ was increased to $V_{cr2\_max}$ = 4968 V to drive the ceramic plate. Also, the TR $n_3$ = 0.05 was used to reduce the voltage to $V_{cr\_sen}$ = 62 V. Passage through the FBCC was used as a condition to protect the system from overvoltage. The waveforms of the voltage and current of the ceramic plate are illustrated in Fig. 4. The ceramic plate had an operational frequency of 46.9 kHz, $v_{cr2\_rms}$ = 301 V, and $i_{cr2\_rms}$ = 1.30 A. The following section describes how the circuit parameters of the FBRI and FBCC were used to design the ATC, and it also describes the mechanism behind the ATC and the regulation of the ammonia gas concentration. By changing the concentration of ammonia gas, the FBRI output power can be controlled, thereby altering the ozone concentration.

$$\omega_o = \frac{\omega_r}{\sqrt{1-\frac{1}{{Q_L}^2}}} \tag{8}$$

$$R_{Load} = \frac{8{V_{in}}^2{\eta_{FBRI}}^2}{\pi^2 P_{Load}\left\{\left[1-\left(\frac{\omega_r}{\omega_o}\right)^2\right]^2+\left[\frac{1}{Q_L}\left(\frac{\omega_r}{\omega_o}\right)\right]^2\right\}} \tag{9}$$

$$L_r = \frac{R_{Load}}{Q_L\omega_o} \tag{10}$$

$$C_r = \frac{Q_L}{\omega_o R_{Load}} \tag{11}$$

$$V_{cr1\_max} = \frac{4V_{in}Q_L}{\pi} \tag{12}$$

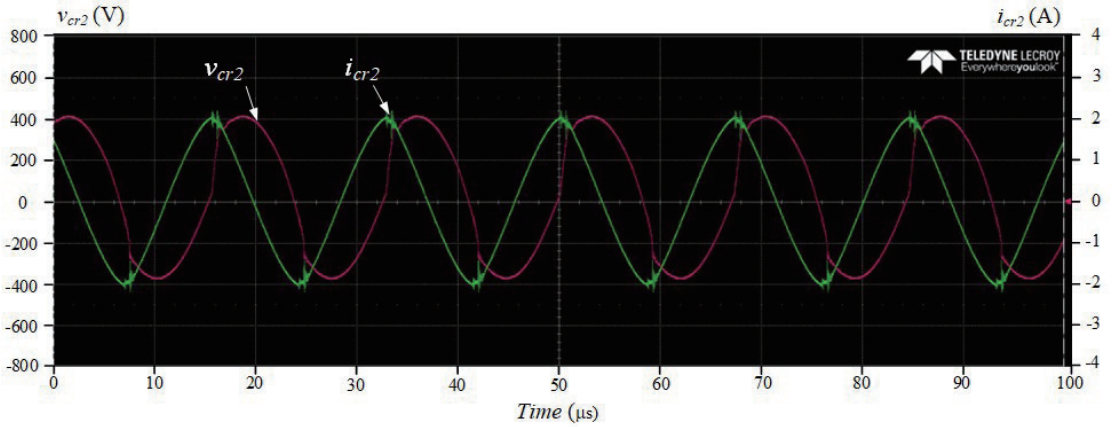


Fig. 4. (Color online) Ceramic plate's $v_{cr2}$ and $i_{cr2}$ waveforms. 200 V/div, 1 A/div, and time: 2.5 µs/div.

### 2.3 ATC operation

From the parameters listed in Table 2, we obtained the operating angular frequency ($\omega_r$), resonance angular frequency ($\omega_o$), and quality factor ($Q_L$). Next, with Eq. (13) obtained from the literature,[20] we calculated $M_v$, which represents the transfer function of the output voltage ($v_{cr1}$) and the input voltage ($v_{in}$). Subsequently, we used different $\omega_r$ / $\omega_o$ ratios to depict changes in $M_v$, thereby determining that when the FBRI is operating at 46.9 kHz, $M_v$ = 6 and $v_{cr1}$ increases sixfold. Because the production of resonance inductance ($L_r$) and resonance capacitance ($C_r$) has an error of ±10%, to avoid marked changes in $v_{cr1}$, 43.8 kHz will not be selected. Because $M_v$ = 6, no marked changes are observed in Fig. 5(a). Therefore, in this study, we altered the range of $M_v$, changing it from 0–800 to 0–30 [Fig. 5(b)], where A, B, C, and D correspond to $P_{out}$ = 100, 75, 50, and 25%, respectively. By increasing the operating frequency ($f_r$) from 46.9 to 49.9 kHz, $M_v$ changed from 6 to 3. By adjusting $v_{cr1}$ from large to small, we adjusted $P_{out}$. By using Eq. (14) from the literature,[19] we determined that A, B, C, and D corresponded to $R_T$ = 4.42, 4.36, 4.28, and 4.17 kΩ, respectively. $R_T$ was used to adjust $P_{out}$.

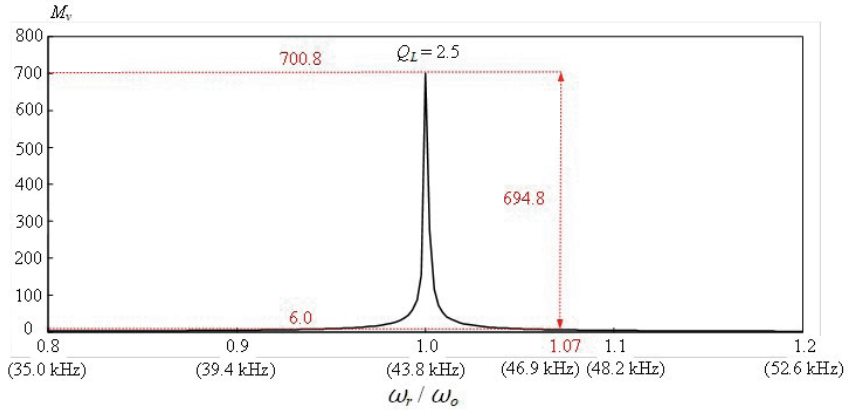


(a)

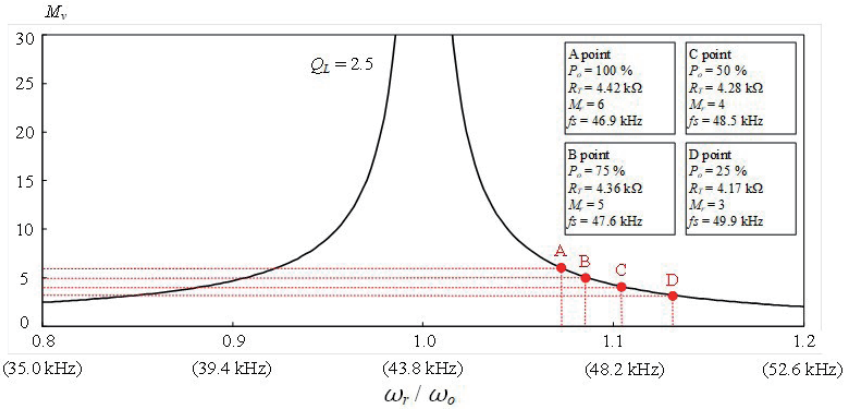


(b)

Fig. 5. (Color online) $M_v$ distributions at different $\omega_r/\omega_o$ values.

In this study, we proposed an ATC (Fig. 6). The goal was to convert the ammonia gas concentration into a voltage signal. By using the voltage signal, we altered $R_T$, adjusted $f_r$, and finally altered $P_{out}$. The ATC consisted of an MQ-137,[22] an operational amplifier ($OPA_1$), comparators ($comp_1$, $comp_2$, and $comp_3$), transistors ($Q_1$, $Q_2$, and $Q_3$), a resister divider ($R_T$), and a PWM circuit . The mechanism is as follows: when the ammonia gas concentration is 100–51 ppm, $OPA_1$ increases the $v_{Ammonia}$ signal sixfold, and $v_{Ammonia1}$ = 2.88 V. Subsequently, the reference voltages of $comp_1$, $comp_2$, and $comp_3$ ($V_{ref1}$, $V_{ref2}$, and $V_{ref3}$) are 2.5, 1.5, and 0.8 V, respectively, all of which are smaller than 2.88 V. Consequently, $Q_1$, $Q_2$, and $Q_3$ are all OFF. At this moment, $R_T$ = 4.42 kΩ, making $P_{out}$ = 100%. When the ammonia gas concentration is 50–31 ppm, $OPA_1$ increases the $v_{Ammonia}$ signal sixfold, and $v_{Ammonia1}$ = 2.34 V. Subsequently, the reference voltage of $comp_1$ ($V_{ref1}$) is greater than 2.34 V. Therefore, $Q_1$ is ON and the short circuit resistance is 60 Ω. $Q_2$ and $Q_3$ are OFF. At this moment, $R_T$ = 4.36 kΩ, making $P_{out}$ = 75%. When the ammonia gas concentration is 30–11 ppm, $OPA_1$ increases the $v_{Ammonia}$ signal sixfold, and $v_{Ammonia1}$ = 1.20 V. Subsequently, the reference voltage of $comp_1$ and $comp_2$ ($V_{ref1}$ and $V_{ref2}$) is greater than 1.20 V. Therefore, $Q_1$ is ON and the short circuit resistance is 60 Ω; $Q_2$ is ON and the short circuit resistance is 80 Ω; and $Q_3$ is OFF. At this moment, $R_T$ = 4.28 kΩ, making $P_{out}$ = 50%. When the ammonia gas concentration is 10–0 ppm, $OPA_1$ increases the $v_{Ammonia}$ signal sixfold, and $v_{Ammonia1}$ = 0.5 V. The reference voltages of $comp_1$, $comp_2$, and $comp_3$ ($V_{ref1}$, $V_{ref2}$, and $V_{ref3}$) are all greater than 0.8 V. Therefore, $Q_1$, $Q_2$, and $Q_3$ are ON, and their short circuit resistances are 60, 80, and 110 Ω, respectively. At this moment, $R_T$ = 4.17 kΩ, making $P_{out}$ = 25%. Because ammonia gas is continually generated in piggeries, the system is generally kept operating at $P_{out}$ = 25%. If the $V_{Ozone}$ feedback signal does not match the actual ozone concentration, the ozone generator has malfunctioned and the system will cease operating. When $R_T$ changes, $I_s$ changes accordingly. As a result, the $f_r$ values of the PWM output signals (PWM_1 and PWM_2) ranged between 46.9 and 49.9 kHz. $I_{DT}$ maintains a dead-time, thereby

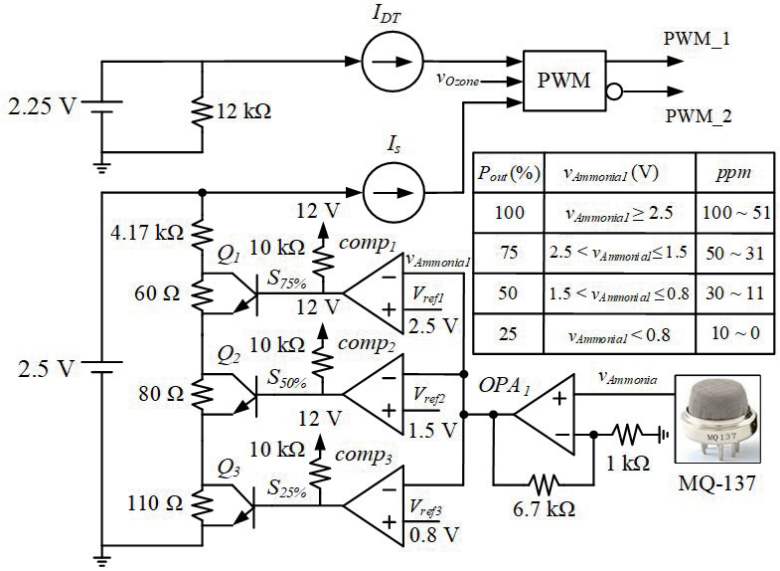


| $P_{out}$ (%) | $v_{Ammonia1}$ (V) | ppm |
|---|---|---|
| 100 | $v_{Ammonia1} \geq 2.5$ | 100 ~ 51 |
| 75 | $2.5 < v_{Ammonia1} \leq 1.5$ | 50 ~ 31 |
| 50 | $1.5 < v_{Ammonia1} \leq 0.8$ | 30 ~ 11 |
| 25 | $v_{Ammonia1} < 0.8$ | 10 ~ 0 |

Fig. 6. (Color online) Measuring ammonia concentrations using ATC.

forming a complementary relationship between PWM_1 and PWM_2 to avoid both PWM_1 and PWM_2 being conducted and resulting in a short circuit.

$$M_v = \frac{v_{cr1}}{v_{in}} = \frac{2\sqrt{2}}{\pi\sqrt{\left[1-\left(\frac{\omega_r}{\omega_o}\right)^2\right]^2 + \left[\frac{1}{Q_L}\left(\frac{\omega_r}{\omega_o}\right)\right]^2}} \tag{13}$$

$$R_T = \frac{(2.5\times 83)}{f_r} \tag{14}$$

## 3. Experimental Ammonia Decomposition Results of DSATAC

In this study, we used the DSATAC to decompose ammonia gas in a three-step process. (1) CPOG output ozone concentrations were generated under different power levels. (2) The effect of decomposing ammonia gas using different output power levels was assessed. (3) The effect of using natural ventilation to decompose ammonia gas was also assessed. In experiments, 1, 2, and 3 mL of ammonia water were used to generate ammonia, which was sent to the washing basket. After using a device to confirm that the ammonia gas concentration was stable, we then measured the decomposition effect. The highest concentration of ammonia gas was 100 ppm, which was within the measuring scope of the MQ-137 detector.

The CPOG used four power levels to drive the ceramic plate. BMT 964 was used to measure ozone concentration. In Fig. 7, the measurement time was 600 s. When $P_{out}$ = 25, 50, 75, and 100%, the corresponding stable ozone concentrations were 31.0, 54.8, 74.0, and 91.6 ppm, respectively. We observed that when $P_{out}$ was increased from 25 to 50%, the ozone concentration

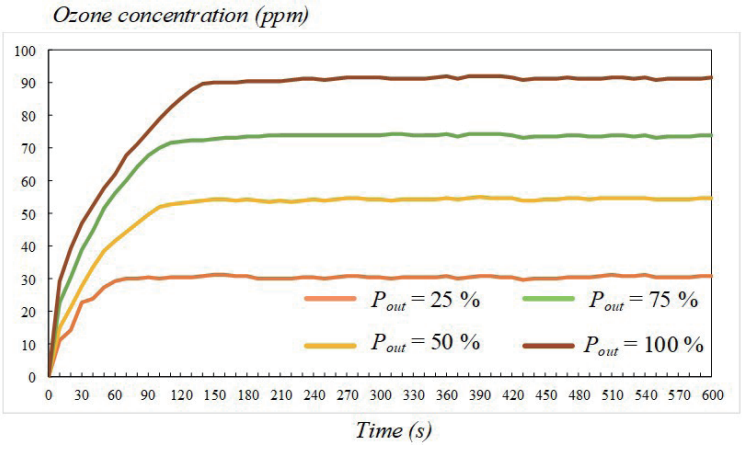


Fig. 7. (Color online) Changes in experimental ozone concentrations under different CPOG output powers.

increased by 23.8 ppm. When $P_{out}$ was increased from 50 to 75%, the ozone concentration increased by 19.2 ppm. When $P_{out}$ was increased from 75 to 100%, the ozone concentration increased by approximately 17.6 ppm.

In the results presented in Figs. 8–10, four different CPOG power levels were used to generate four different ozone concentrations to decompose the ammonia gas generated by 1, 3, and 5 mL of ammonia water. The time required for the ammonia gas concentrations to be reduced from 100 to 0 ppm was recorded. In this study, we proposed Eq. (15) to calculate the decomposition ratio so as to assess the effectiveness of different concentrations of ozone in decomposing ammonia gas. In Eq. (15), the decomposition ratio ($DR_{mL\_Po}$) is a percentage. $AC_{100\ ppm}$ indicates an ammonia gas concentration of 100 ppm. The ammonia gas concentration after 60 s is indicated by $AC_{60\ s}$.

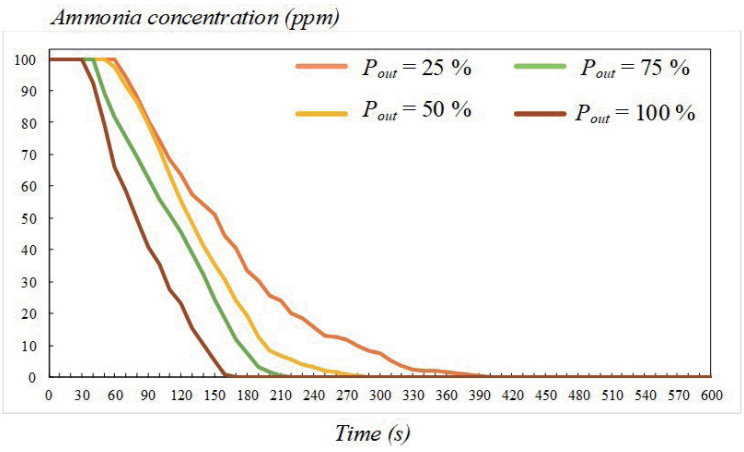


Fig. 8. (Color online) Changes in experimental ammonia concentrations in 1 mL of ammonia water under different CPOG output powers.

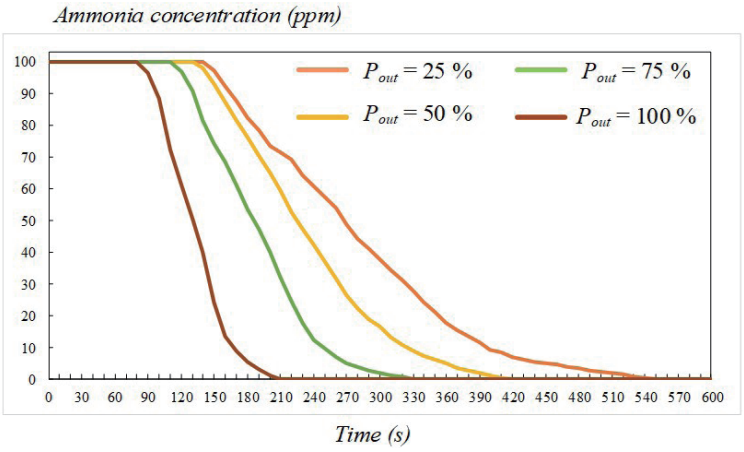


Fig. 9. (Color online) Changes in experimental ammonia concentrations in 3 mL of ammonia water under different CPOG output powers.

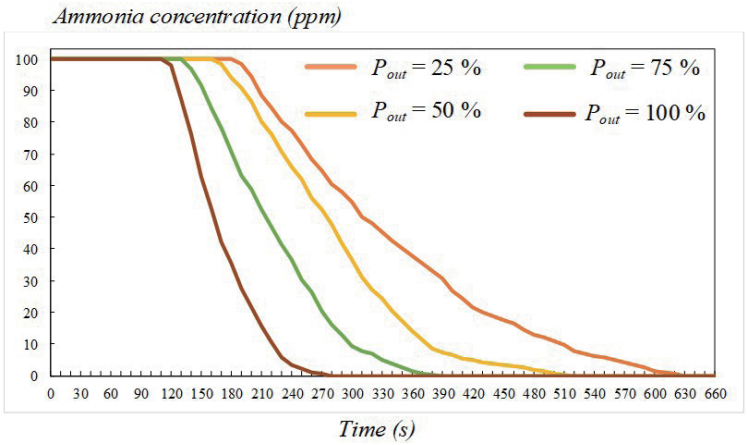


Fig. 10. (Color online) Changes in experimental ammonia concentrations in 5 mL of ammonia water under different CPOG output powers.

$$DR_{mL\_Po}(\%) = \frac{\left(AC_{100\ ppm} - AC_{60\ s}\right)}{AC_{100\ ppm}} \times 100\% \tag{15}$$

In Fig. 8 (1 mL of ammonia water), when $P_{out}$ = 25, 50, 75, and 100%, the durations required for the ammonia concentration to be reduced from 100 to 0 ppm were 400, 300, 220, and 170 s, and the corresponding decomposition ratios were $DR_{1mL\_25\%}$ = 36.2%, $DR_{1mL\_50\%}$ = 36.4%, $DR_{1mL\_75\%}$ = 44.0%, and $DR_{1mL\_100\%}$ = 58.9%, respectively. In Fig. 9 (3 mL of ammonia water), when $P_{out}$ = 25, 50, 75, and 100%, the durations required for the ammonia concentration to be reduced from 100 to 0 ppm were 530, 420, 330, and 200 s, and the corresponding decomposition ratios were $DR_{3mL\_25\%}$ = 26.8%, $DR_{3mL\_50\%}$ = 29.7%, $DR_{3mL\_75\%}$ = 38.8%, and $DR_{3mL\_100\%}$ = 60.2%, respectively. In Fig. 10 (5 mL of ammonia water), when $P_{out}$ = 25, 50, 75, and 100%, the durations required for the ammonia concentration to be reduced from 100 to 0 ppm were 630, 520, 390, and 280 s, and the corresponding decomposition ratios were $DR_{5mL\_25\%}$ = 22.6%, $DR_{5mL\_50\%}$ = 23.7%, $DR_{5mL\_75\%}$ = 36.8%, and $DR_{5mL\_100\%}$ = 57.7%, respectively.

According to the decomposition ratios from Figs. 8–10, when $P_{out}$ = 25%, a fixed ozone concentration was input to the washing basket. As the concentration of ammonia gas increased, the decomposition ratio became 36.2, 26.8, and 22.6%, and additional time was required to decompose 3 and 5 mL of ammonia gas to 0 ppm. To reduce the duration, the ozone concentration must be increased. The same phenomenon was observed when the system was operating at $P_{out}$ = 50 and 75%. When $P_{out}$ = 100%, the decomposition ratios corresponding to the increase in the concentration of ammonia gas were 58.9, 60.2, and 57.7%. The decomposition ratio increased from 58.9 to 60.2%, indicating that the ozone concentration did not have to increase further. When the decomposition ratio reached 57.7%, for 5 mL of ammonia gas, the ozone concentration required additional time to reduce to 0 ppm. To reduce the duration, the ozone concentration must be increased. As shown in Fig. 11, complete natural ventilation was adopted to decompose 1, 3, and 5 mL of ammonia gas. The duration required for reducing the ammonia gas

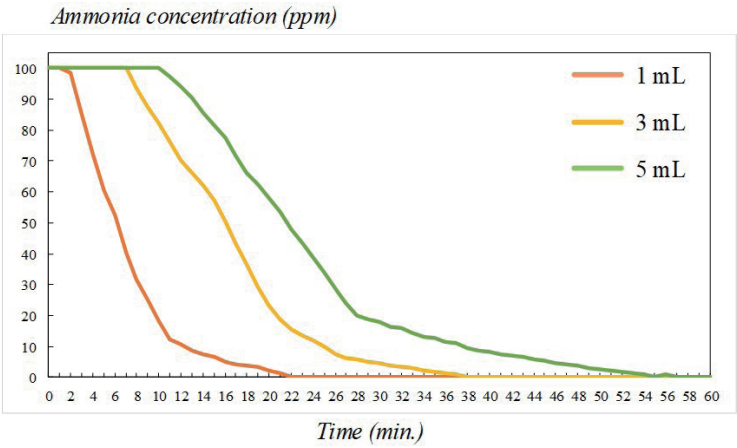


Fig. 11. (Color online) Changes in experimental ammonia concentrations in natural ventilation.

Table 4
Ammonia decomposition times obtained using different decomposition methods.

| Decomposition method | Ammonia water | | | Unit |
|---|---|---|---|---|
| Natural ventilation | 1 | 3 | 5 | mL |
| | 22 | 38 | 56 | min |
| Combined use of ozone and water spray for decomposition | | | | |
| Ozone concentration ($P_o$ = 25%) | 400 | 530 | 630 | s |
| Ozone concentration ($P_o$ = 50%) | 300 | 420 | 520 | ppm |
| Ozone concentration ($P_o$ = 75%) | 220 | 330 | 390 | ppm |
| Ozone concentration ($P_o$ = 100%) | 170 | 220 | 280 | ppm |

concentration from 100 to 0 ppm was measured. It was determined that 22, 38, and 56 min were required to reduce the concentration to 0 ppm. Table 4 organizes the data on ammonia gas decomposition presented in Figs. 8–10, demonstrating that when the output ozone concentration from the ozone generator was higher, ammonia decomposed more quickly.

## 5. Conclusions

In this study, we proposed a DSATAC that uses an ATC to transform the ammonia gas concentration into a voltage signal. The ARC mechanism first alters $R_T$, then adjusts the $f_r$ of the FBRI, and subsequently controls the $P_{out}$ of the FBRI to be 100, 75, 50, or 25%. The corresponding ozone concentrations are 91.6, 74.0, 54.8, and 31.0 ppm, respectively.

When $P_{out}$ = 100%, the CPOG generated 91.6 ppm of ozone with water mist to decompose ammonia gas. The experimental results demonstrated that when ammonia water of 1, 3, and 5 mL volumes generated ammonia gas, durations of 170, 220, and 280 s were required to reduce the concentration of ammonia gas from 100 to 0 ppm. The decomposition ratios were 58.9, 60.2, and 57.7%, respectively. An increase in decomposition ratio from 58.69 to 60.2% indicated that the ozone concentration was suitable. When the decomposition ratio reached 57.7%, the ozone

required additional time to decompose the ammonia gas from 5 mL of ammonia water to 0 ppm. To reduce this duration, the ozone concentration must be increased. When using natural ventilation, 22, 38, and 56 min were required to reduce the ammonia concentration to 0 ppm. Therefore, the DSATAC can quickly decompose ammonia gas. The ATC can also be applied to detect other gases.

## Acknowledgments

This research was funded by the Ministry of Science and Technology (NO. MOST 109-2622-E-150-025).

## References

1 D. M. Miles, W. W. Miller, S. L. Branton, W. R. Maslin, and B. D. Lott: Avian Dis. **50** (2006) 45. https://doi.org/10.1637/7386-052405R.1
2 C. J. Phillips, M. K. Pines, M. Latter, T. Muller, J. C. Petherick, S. T. Norman, and J. B. Gaughan: Anim. Sci. **88** (2010) 3579. https://doi.org/10.2527/jas.2010-3089
3 M. Neghab, A. Mirzaei, F. Kargar Shouroki, M. Jahangiri, M. Zare, and S. Yousefinejad: Ind. Health **56** (2018) 427. https://doi.org/10.2486/indhealth.2018-0014
4 Y. Nakata, R. Mabuchi, K. Teranishi, and N. Shimomura: IEEE Trans. Dielectr. Electr. Insul. **20** (2013) 1146. https://doi.org/10.1109/TDEI.2013.6571429
5 K. P. Shine: Ozone Sci. Eng. **23** (2001) 429. https://doi.org/10.1080/01919510108962026
6 W. Wang, L. Flynn, X. Zhang, Y. Wang, Y. Wang, F. Jiang, Y. Zhang, F. Huang, X. Li, R. Liu, Z. Zheng, W. Yu, and G. Liu: IEEE Trans. Geosci. Remote Sens. **50** (2012) 4943. https://doi.org/10.1109/TGRS.2012.2210902
7 O. A. Nashmia, A. A. Mohammeda, and N. N. Abdulrazzaqb: Iraqi J. Chem. Pet. Eng. **21** (2020) 25. https://doi.org/10.31699/IJCPE.2020.2.4
8 D. A. Vargas, D. E. Casas, D. R. Chávez-Velado, R. L. Jiménez, G. K. Betancourt-Barszcz, E. Randazzo, D. Lynn, A. Echeverry, M. M. Brashears, M. X. Sánchez-Plata, and M. F. Miller: Foods **10** (2021) 1. https://doi.org/10.3390/foods10092106
9 T. Batakliev, V. Georgiev, M. Anachkov, S. Rakovsky, and G. E. Zaikov: Interdiscip. Toxicol. **7** (2014) 47. https://doi.org/10.2478/intox-2014-0008
10 K. E. Lamb, M. D. Dolan, and D. F. Kennedy: Int. J. Hydrog. Energy. **44** (2019) 3580. https://doi.org/10.1016/j.ijhydene.2018.12.024
11 Y. Shifeng and L. Yajuan: Proc. 2013 2nd Int. Symp. Computer, Communication, Control and Automation Conf. (2012) 171–174.
12 M. A. Putra, M. Rivai, and A. Arifin: Proc. 2018 IEEE Int. Seminar on Intelligent Technology and Its Applications Conf. (IEEE, 2018) 409–412.
13 M. Rivai, Misbah, M. Attamimi, M. H. Firdaus, Tasripan, and Tukadi: Proc. 2019 IEEE Int. Conf. Computer Engineering, Network, and Intelligent Multimedia (IEEE, 2019) 1–5.
14 T. Fujishima: J. Int. Counc. Electr. Eng. **8** (2018) 99. https://doi.org/10.1080/22348972.2018.1477089
15 T. Fujishima, T. Kawaguchi, T. Amano, and T. Yamashita: Proc. 2013 3rd Int. Conf. Electric and Electronics (EEIC, 2013) 1–4
16 N. Hammadi, M. Zegrar, S. Nemmich, Z. Dey, S. Remaoun, B. Naouel, and A. Tilmarine: J. Eng. Sci. Technol. **11** (2016) 755. https://www.semanticscholar.org/me/research
17 A. M. Lopez, H. Piquet, D. Patino, R. Diez, and X. Bonnin: IEEE Trans. Plasma Sci. **41** (2013) 2335. https://doi.org/10.1109/TPS.2013.2273462
18 Datasheet of UCC27712: https://www.ti.com/lit/ds/symlink/ucc27712.pdf (accessed March 2020).
19 Datasheet of UCC25600: https://www.ti.com/lit/ds/symlink/ucc25600.pdf (accessed June 2015).
20 Datasheet of UCC28019: https://www.ti.com/lit/ds/symlink/ucc28019.pdf (accessed April 2007).
21 K. K. Marian and C. Dariusz: Resonant Power Converters (Wiley, NY, USA, 2011) 2nd ed., Chap. 7.
22 MQ-137 Gas Sensor: https://www.meterkala.com/media/uploads/files/products/MQ137.pdf (accessed March 2015).

## About the Authors

**Sheng-Yi Tang** received his B.S. degree from Kao Yuan University, Taiwan, R.O.C., in 2002 and his M.S. and Ph.D. degrees from National Sun Yat-sen University, Taiwan, R.O.C., in 2004 and 2010, respectively. Since 2018, he has been an assistant professor at National Formosa University, Taiwan, R.O.C. His research interests are in power electronics, modern control technology, and ozone.

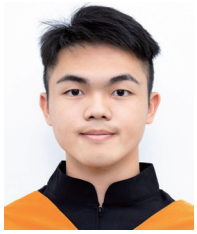

**Yu-Hao Hu** received his B.S. degree from National Formosa University, Taiwan, R.O.C., in 2017 and his M.S. degree from National Formosa University, Taiwan, R.O.C., in 2021. His research interests are in modern control technology and ozone.